Stochastic Inversion of geophysical data by sequential Bayesian updating under a non-stationary Gaussian process prior

Jef Karel Caers [1], Peng Li [1], Jonas Kloeckner[1], Juan Pablo Daza[1], David Zhen Yin[1] and Céline Scheidt [2,*]

[1] Departments of Earth & Planetary, Stanford University, USA;
[2] Department of Energy Science Engineering, Stanford University, USA;

"Peng Li" <pli6@stanford.edu>; "Jonas Kloeckner" <jkloeckn@stanford.edu>; "David Zhen Yin" <yinzhen@stanford.edu>; "Juan Pablo Daza" <jpdaza@stanford.edu>; "Celine Scheidt" <scheidtc@stanford.edu>; "Jef Karel Caers" jcaers@stanford.edu

Stochastic Inversion of geophysical data by sequential Bayesian updating under a non-stationary Gaussian process prior

Jef Karel Caers [1], Peng Li [1], Jonas Kloeckner[1], Juan Pablo Daza[1], David Zhen Yin[1] and Céline Scheidt [2,*]

[1] Departments of Earth & Planetary, Stanford University, USA;
[2] Department of Energy Science Engineering, Stanford University, USA;
* Correspondence: scheidtc@stanford.edu;

Abstract

The acquisition of geophysical data is becoming increasingly important in the context of critical mineral exploration. Geophysical data and inversion product are essential to map many components of the critical mineral system by detecting geophysical anomalies that can be interpreted by expert geologists. However, the inversion of airborne geophysical data acquired along flightlines into subsurface petrophysical properties remains an outstanding challenge. Many inversion techniques rely either on 1D deterministic inversion or on stochastic inversion on a local scale. The outcome of our work is the stochastic inversion along flightlines of 2D panels (flightline direction vs depth), while at the same time producing plausible spatial variation of the petrophysical properties. Our method relies on a sequential application of Bayesian inversion, where we invert a sequence of 2D panels such that the variation of petrophysical properties avoid generation of artifacts across the panel boundaries. We show that our method can be used in a practical setting in the context of mineral exploration in the Cape Smith Belt of Canada.

Keywords: geophysical inversion, Gaussian processes, sequential Bayes, uncertainty quantification, critical minerals

1. Introduction

In the drive to explore for critical minerals needed for the energy transition, many countries have been or are in pursuit of mapping the subsurface using large spread airborne geophysics. Typically, several types of geophysical measurements are obtained such as gravity, magnetic, and EM. Data along flightlines is then interpolated to obtain a 2D (or time-domain in EM) map of measured magnetic, gravity and EM. These maps are used to detect geophysical anomalies of interest; they may be used in mineral prospectivity mapping or may guide exploration companies in drilling certain targets.

In addition, the data contains information on the variation of petrophysical properties in the 3D subsurface. Inversion is used to turn the geophysical signals into 3D models of the subsurface, either using deterministic or stochastic inversion. This is usually done over areas of particular interest, which tend to be limited in extend. Stochastic inversion along extensive flightlines are not common. Some methods are used in the context of scientific studies of the Earth crusts. Other methods rely on consecutive pseudo-1D or 2D inversions along flightlines [1–3]. These approaches are often deterministic [4]. “2.5-D inversion”, or stacking the same 2D petrophysical models into 3D, is sometimes used by assuming petrophysical homogeneity perpendicular to the lines [5]. Some recent studies in large-scale potential field inversion were conducted directly on 3D voxel models with regularization [6]. Similarly, [7] attempted to invert the 3D conductivity of the contiguous US on a 70-km grid mesh from magneto-telluric (MT) data. All above results were obtained by minimizing the misfit between model-predicted geophysical maps and the observed data (often interpolated) with a model parameter regularization term, using gradient-based optimization. In these approaches, a well-defined large-scale 2D/3D reference (or initial model) is essential, often with weights used to control how the inverted results closely adhere to the reference model [8]. The resulting models are typically deterministic, and defining 3D reference models at large scales can be very difficult. What is lacking today are methods that can perform stochastic inversions along flightline data. While this work does not yet cover very large areas, such as entire countries, it proposes a method that can be extended to large scale applications.

Several challenges need to be overcome to achieve this. A single-step inversion over a large area is not feasible in terms of memory and computational resources, as well as the challenge of formulating a single prior model. To address this, we will perform stochastic inversions per panel,

along the direction of the flightline, making sure that panels are stitched together without creating artificial boundaries. Secondly, the spatial variability of the petrophysics properties may change dramatically over large distances due to changes in rock formations (ages) and the existence of faulting structures. This means that the style of spatial variability of these physical properties is likely to change in their direction of continuity (e.g. azimuthal and dipping) and in their subsurface morphologies (layers, intrusions, folding). This means that building comprehensive prior distribution models for multiple petrophysical properties required for Bayesian inversion is challenging. To address this issue, we use non-stationary Gaussian processes as prior, where the non-stationary mean and covariance function are also uncertain, i.e. have their own prior distributions. We intend to show that with these non-stationary Gaussian priors, a wide range of possible petrophysical variations can be generated. Additionally, correlation structures related to large-scale geological structures between the various petrophysical properties can be imposed. Our approach is applied to the Cape Smith Belt, which is currently under exploration for Ni-Cu-Co sulfide deposits.

2. Application area

Our area of study is from the Cape Smith Belt (CSB) in Nunavik region of northern Québec, Canada. As an early Proterozoic thrust belt containing metamorphosed basaltic volcanic, mafic intrusive, and sedimentary rocks, the CSB has been widely explored for Ni-Cu-PGE magmatic sulfide deposits. We will use the recently acquired HeliTEM magnetic data in this area provided from Geomining Information System of Quebec, published to the public domain by KoBold Metals [9]. The HeliTEM magnetic data were flown by Xcalibur Smart Mapping between June 18 and August 24, 2022, with survey coverage consisting of 3626.0 km of traverse lines flown with a spacing of 200 m and 381.7 km of tie lines ranging between 1450 and 2000 m spacing for a total of 4007.7 km (Figure 1).

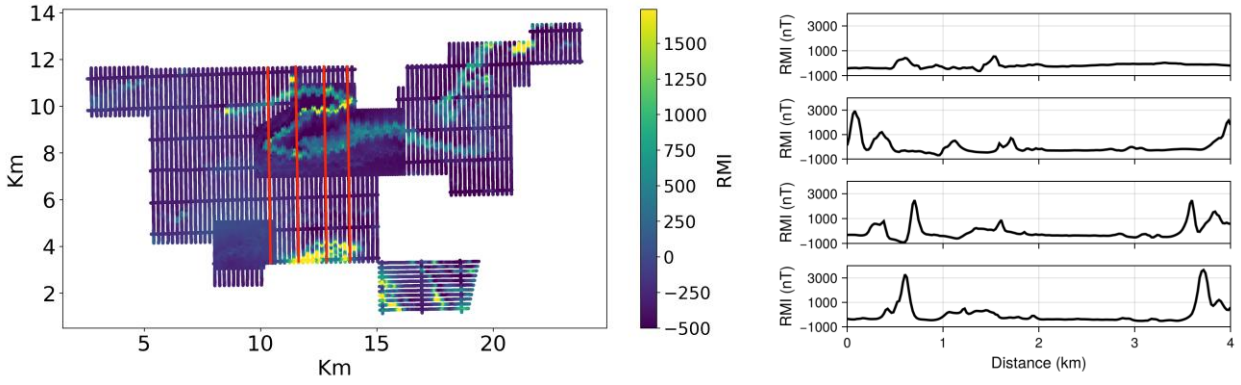

Figure 1: HeliTEM magnetic data acquired in the Cape Smith belt. We will focus on the 4 red lines

3. Methodology

3.1. Sequential Bayesian updating: a review

Our approach aims to solve a larger inverse problem by the sequential inversion of smaller panels, areas or blocks. Since the approach is Bayesian, we will review here some fundamental concepts of sequential Bayesian updating. Consider a model parameter y that is informed by a sequence of data $x_1, x_2, \dots, x_n$. In a Bayesian context we start with a prior distribution $p(y)$ and at step n, we can decompose the likelihood as follows:

$$p(x_1, x_2, \dots, x_n|y) = p(x_1|y)p(x_2|x_1, y) \dots p(x_n|\mathbf{x}_{n-1}, y) \tag{1}$$

Defining

$$\mathbf{x}_{n-1} = \{x_{n-1}, x_{n-2}, \dots, x_1\} \tag{2}$$

The update distribution at time n then is the posterior

$$p(y|\mathbf{x}_n) = p_n(y) \sim p(y)\, p(\mathbf{x}_n|y) \tag{3}$$

Then, after obtaining new information x_{n+1}, we start anew and update

$$p_{n+1}(y) = p(y|\mathbf{x}_{n+1}) \sim p(y)\, p(\mathbf{x}_{n+1}|y)$$

(4)

Essentially, we are using the $p_n(y)$ as the prior distribution in the next step of the Bayesian update to get the next posterior $p_{n+1}(y)$. Indeed, we can derive that the posterior of y at step n become the prior at step $n+1$

$$p_n(y)p(x_{n+1}|\mathbf{x}_n, y) = p(y)p(\mathbf{x}_n|y)p(x_{n+1}|\mathbf{x}_n, y) = p(y)p(\mathbf{x}_{n+1}|y) \sim p_{n+1}(y)$$

(5)

Note that we do not need a conditional independence assumption in this derivation. The revised posterior equals the current posterior times the likelihood of the new data. All historical knowledge about y is captured by $p_n(y)$. The sequential application of Bayes' rule is therefore recursive.

Consider now a problem with a dynamic y, changing in time (or in space, or both), and a Markovian (conditional independence) model is used

$$p(y_{n+1}|\mathbf{y}_n) = p(y_{n+1}|y_n)$$

(6)

where $\mathbf{y}_n = \{y_n, y_{n-1}, .., y_1\}$.

The true state is not observed; instead, a sequence of data is acquired. Assuming conditional independence:

$$p(x_n|\mathbf{y}_n, \mathbf{x}_{n-1}) = p(x_n|y_n)$$

(7)

Then the joint density becomes

$$p(\mathbf{x}_n, \mathbf{y}_n) = p(y_0) \prod_{i=1}^{n} p(y_i|y_{i-1})p(x_i|y_i)$$

(8)

The dynamic evolution of y is modeled using two steps: predict y at time n from data at previous times (filter step) and predict a y at the next step, $n+1$. The filter distribution is the posterior $p(y_n|\mathbf{x}_n)$. Using this filter distribution, the predictive distribution becomes

$$p(y_{n+1}|\mathbf{x}_n) = \int_{y_n} p(y_{n+1}|y_n)\, p(y_n|\mathbf{x}_n)\, dy_n \tag{9}$$

After a new observation x_{n+1} is obtained, application of recursive Bayes combines the predictive distribution with a new likelihood $p(x_{n+1}|y_{n+1})$:

$$p(y_{n+1}|\mathbf{x}_{n+1}) = p(y_{n+1}|x_{n+1}, \mathbf{x}_n) = p(y_{n+1}|\mathbf{x}_n)\, p(x_{n+1}|y_{n+1}) \tag{10}$$

Where now x_{n+1} is conditionally independent $\mathbf{x}_n$, knowing y_{n+1}. This formulation looks deceivingly simple because calculating high-dimensional pdfs and dealing with non-linear dynamics requires Monte Carlo simulations. Common approaches are the use of sequential Monte Carlo methods such as particle filtering. However, we will show in the next section that such methods become difficult to apply in a large-scale spatial context where the model and data are both high-dimensional, and the physical model is CPU demanding.

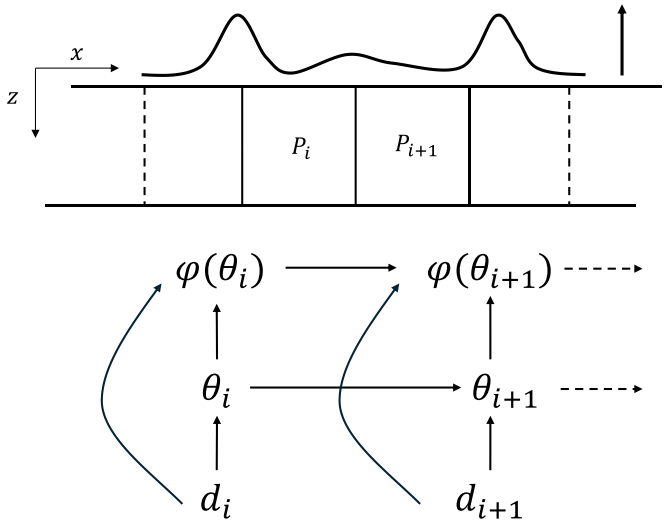

Figure 2: sequential Bayesian formulation for a large-scale geophysical inverse problem.

3.2. A Bayesian formulation for large-scale geophysical inversion

To model large areas, we divide the area over which data needs to be inverted as block (3D), or here as 2D panels (in x and z direction), see Figure 2. For each block we assume the prior to be a Gaussian process but with unknown covariance and mean function. Let φ be a stationary Gaussian process, then for each panel P_i we have

$$\varphi_i = \varphi(s), s \in P_i \tag{11}$$

A stationary Gaussian process is fully defined by stationary mean and covariance

$$E[\varphi(s)] = \mu$$

$$Cov\left(\varphi(s_i), \varphi(s_j)\right) = E\left[(\varphi(s_i) - \mu)(\varphi(s_j) - \mu)\right] = C(s_i - s_j) \tag{12}$$

with C any positive definite function, and where the random vector of any set of location

$$\boldsymbol{\varphi} = \{\varphi(s_1), \varphi(s_2), \dots, \varphi(s_n)\} \tag{13}$$

is multivariate Gaussian

$$\varphi \sim \frac{1}{(2\pi)^{n/2}|\Sigma|^{1/2}} \exp\left(-\frac{1}{2}(\boldsymbol{\varphi} - \boldsymbol{\mu})^T \Sigma^{-1} (\boldsymbol{\varphi} - \boldsymbol{\mu})\right)$$

$$\Sigma_{ij} = C(s_i - s_j) \tag{14}$$

If we consider the mean and covariance function to be the (hyper)-parameters θ of the stationary process, then we can introduce the notation $\varphi_i(\theta_i)$.

Figure 2 shows the sequential Bayesian model that applies to this case. In comparison with the notation of the previous section, we have $y = \{\varphi, \theta\}$ and the $x = d$, the geophysical data. The difficulty in applying the sequential approach to our problem is that

- φ represents a process in space and is high-dimensional.
- θ that defines the process φ is unknown.
- The relationship between θ and d is not known/intractable.
- The relationship between φ and d is known but not linear.
- Spatial dependency exists between φ_n and φ_{n+1} as well as θ_n and θ_{n+1}.

Still, we can apply the "predict plus filter" approach to this problem:

- *Predict*: sample the posterior distribution of the next panel P_{i+1}, given the previous panel P_i. This will require enforcing spatial correlation between φ_n and φ_{n+1} as well as θ_n and θ_{n+1}.
- *Filter*: sample the posterior distribution of the next panel, given the geophysical data of the next panel. This requires solving an inverse problem using the geophysical data of the next panel and the predictive distribution as the prior distribution (relying on the recursive Bayes model).

Consider the first panel P_0. In the first step, using the (stated) prior distribution:

$$p(\theta_0, \varphi_0) = p(\theta_0)\, p(\varphi_0|\theta_0) \tag{15}$$

we sample several realizations of θ_0 then of φ_0, creating realizations $(\theta_0, \varphi_0)_i, i = 1, \dots, L$. In the next step, we need to filter the geophysical data d_0, in other words solve an inverse problem. Solving such problem requires sampling from $p(\theta_0, \varphi_0|d_0)$. This problem is treated in section 3.3. After inversion, the next set of particles $(\theta_1, \varphi_1)_i$ need to be predicted from the updated set $(\theta_0, \varphi_0)_i$. The relationship between φ_1 and φ_0 is linear, since they model the same property. In geostatistical jargon, any realization of φ_0 serves as hard/exact data for constraining the Gaussian process φ_1. At the same time, we need to sample θ_1, given θ_0. This problem is treated in section 3.4. Then this procedure is recursively applied until all panels have been inverted.

Our approach will use Monte Carlo simulation, but does not employ particle filtering, meaning that we sample directly from the posterior distribution without employing an importance sampler. Instead, we leverage high-performance computing to generate an ensemble of inverted models, computed in parallel. Next, we will detail both filter and predict step.

3.3. Filter: Inversion of a single panel

We now focus on the filtering aspect of our sampler. θ and φ need to be inverted (filtered) sequentially, honoring the hierarchical relationship between them. To do so, we propose the following decomposition of the joint inversion of θ and φ at step n

$$p(\theta_n, \varphi_n|d_n) = p(\theta_n|d_n)\, p(\varphi_n|d_n, \theta_n)$$

(16)

Consider first $p(\theta|d)$ whose dimension is low. For example, in 2D, the Gaussian process has a maximum of three parameters for the covariance function (one angle and two ranges) and a mean and variance, which is a total of five parameters. This suggests modeling $p(\theta|d)$ as a high-dimensional density function. To estimate this density function we generate a training set by Monte Carlo simulation, then estimate $p(\theta|d)$, then sample from the estimated distribution with an exact method. More specifically consider the joint distribution:

$$p(\theta_n, d_n) = p(\theta_n)p(d_n|\theta_n) = p(\theta_n)p(d_n|\varphi_n)p(\varphi_n|\theta_n)$$

(17)

using the Bayes' network definition (Figure 2) in the last step, where d_n is related to θ_n, through the spatial model φ_n. To sample a joint distribution $p(\theta, d)$ for any panel (n), we therefore perform the following sequential sampling:

$$\theta^{(j)} \sim p(\theta)$$

(18)

then sample a Gaussian process realization:

$$\varphi^{(j)} \sim p(\varphi\,|\theta^{(j)})$$

(19)

then forward model the data:

$$d^{(j)} = g(\varphi^{(j)})$$

(20)

Note that we use superscript (j) to indicate a sample, while using a subscript to indicate a panel. We now have the training dataset:

$$\{\theta^{(j)}, d^{(j)}\}, j = 1, \dots, J$$

(21)

The training set is used to fit a high-dimensional probability density model $\hat{p}(\theta, d)$, from which a conditional distribution can be calculated:

$$\hat{p}(\theta|d) = \frac{\hat{p}(\theta, d)}{\hat{p}(d)}$$

(22)

For the second term $p(\varphi|\theta, d)$, we need to solve a non-linear inverse problem with Gaussian prior whose hyperparameters are known. In Appendix A we review a known solution for this problem through the probability perturbation method. This method was implemented leveraging the fast Fourier transformation for Gaussian process simulation through the Julia package GeoStats [10–12].

3.4. Predict: generating a new prior

At this stage we need a predictive distribution that generates a new prior for the next inversion. Practically speaking, at this stage we have a set of realizations of the previous panel that match the geophysical data of that panel. Following eq.15 of the predictive model, we need to specify $p(\varphi_{n+1}, \theta_{n+1}|\varphi_n, \theta_n)$, which can be further decomposed as

$$p(\varphi_{n+1}, \theta_{n+1}|\varphi_n, \theta_n) = p(\varphi_{n+1}|\varphi_n, \theta_n, \theta_{n+1})\, p(\theta_{n+1}|\varphi_n, \theta_n)$$

(23)

The first term is the distribution of a Gaussian process conditioned to a previously sampled Gaussian process in panel P_n, with known covariance parameters. This is a solved problem in

geostatistics known as conditional simulation under a Gaussian model, for which several sampling algorithms are available, such as sequential Gaussian simulation (Wang et al, 2024).

In the second term, we need to impose spatial continuity between the hyperparameters. First, we assume conditional independence

$$p(\theta_{n+1}|\theta_n, \varphi_n) \cong p(\theta_{n+1}|\theta_n) \tag{24}$$

to determine $p(\theta_{n+1}|\theta_i)$ we consider that θ_{n+1} depends on θ_n, because the data d_{n+1} is correlated to d_n. In section 3.3, we saw how we can estimate both $p(\theta_n|d_n)$ and $p(\theta_{n+1}|d_{n+1})$. We therefore approximate $p(\theta_{i+1}|\theta_i)$ using a distribution $p^*(\theta_{i+1}|\theta_i)$ estimated from samples $\theta_i^*, \theta_{i+1}^*$ as follows:

$$p(\theta_{i+1}|\theta_i) \cong p^*(\theta_{i+1}|\theta_i) \quad \text{with} \quad \theta_i^* \sim p(\theta_i|d_i) \; and \; \theta_{i+1}^* \sim p(\theta_{i+1}|d_{i+1}) \tag{25}$$

3.5. Complete methodology

Our method is a Monte Carlo method, meaning that each spatial model that matches all the geophysical data is sampled independently. We do not employ a particle filter where an ensemble model is updated jointly. As outlined in the previous section, there are methodological challenges that make application of particle filtering challenging. Additionally, leveraging parallel computing, we can run each sample on a different GPU/CPU. With 100 cores, the cost of 100 samples is the same as one sample. A naïve Monte Carlo method is also much more straight forward to implement compared to a particle filter, which requires the additional modeling of an importance sampler, which is not trivial when dealing with spatial models.

Algorithm 1 summarizes, using the above notations, the various steps of the process which are:

- Estimating a predictive model for the hyper-parameters of the Gaussian process
- Iterative application of the Filter & Predict steps

Algorithm 1: the proposed algorithm, $\hat{p}$ is calculated using Eq. 22, p^* is calculated using Eq. 25.

Input	Prior $p(\theta_0)$, $p(\varphi_0|\theta_0)$
	Geophysical data per panel: $d_{obs,0}, d_{obs,1}, \dots, d_{obs,n}$
Output	Posterior samples $(\varphi_{0,post}, \theta_{0,post}), (\varphi_{1,post}, \theta_{1,post}), \dots, (\varphi_{n,post}, \theta_{n,post})$
Estimate a predictive model for Gaussian process hyperparameters (training set)	
	Sample: $\theta^{(j)} \sim p(\theta_0)$; $\varphi^{(j)} \sim p(\varphi_0|\theta_0), j = 1, \dots, J$
	Calculate: $d^{(j)} = g(\theta^{(j)}), j = 1, \dots, J$
	Estimate: $\hat{p}(\theta|d)$ using samples $(\theta^{(j)}, d^{(j)}), j = 1, \dots, J$
	Sample $\theta_0^{*,(j)} \sim p(\theta_0|d_0)$ *and* $\theta_1^{*,(j)} \sim p(\theta_1|d_1), j = 1, \dots, J$
	Estimate: $p^*(\theta_1|\theta_0)$ using samples $(\theta_0^{*,(j)}, \theta_1^{*,(j)}), j = 1, \dots, J$
Do Panel 0	
	Predict: $\theta_{0,obs} \sim \hat{p}(\theta|d_{obs,0})$; $\varphi_{0,obs} \sim p(\varphi_0|\theta_0)$
	Filter: $\varphi_{0,post} \sim p(\varphi_0|d_{obs,0}, \theta_{0,obs})$ using probability perturbation
For Panel $i = 1, \dots, n$	
	Predict $\theta_{i,obs}^* \sim p^*(\theta_i|\theta_{i-1})$; $\varphi_{i,obs} \sim p(\varphi_i|\varphi_{i-1}, \theta_i)$
	Filter: $\varphi_{i,post} \sim p(\varphi_i|d_{obs,i}, \theta_{i,obs})$ using probability perturbation
End	Repeat starting with Panel 0

Prior variables		Definition	Distributions
Gaussian process hyper-parameters 2D anisotropy	a	Length of the semi-major axis of ellipse, in meters	$U[200, 700]$
	b_f	Length ratio of the semi-minor axis to the semi-major axis in an ellipse, the length of semi-minor axis $b = ab_f$	$U[0.01, 1]$
	γ	Azimuth angle of ellipse	$U[1, 180]$
Petrophysics	μ_{ms}	Mean value magnetic susceptibility	$U[0, 0.3]$
	σ_{ms}	Standard deviation magnetic susceptibility	$U[0.05, 0.5]$

Table 1: A broad prior distribution on model variables, as an initial statement of uncertainty. This prior needs to be tested, in a falsification test, with actual observed data.

4. Application

4.1 Illustration of a two-panel case

4.1.1. Falsification test for the prior $p(\theta_0)$

Before moving to the full real case, we present in detail the application of the above methodology to a two-panel case: predict and filter. Application to multiple panels is then the sequential application of the two-panel solution. Before starting the iterative filter, we need to generate a training set for predicting the conditional hyperparameter distribution, $\hat{p}(\theta|d)$, and derive from this $p^*(\theta_{i+1}|\theta_i)$. The training set should be able to predict the data along a line, in other words, a falsification test is needed on the prior distribution $p(\theta_0)$, see Figure 3. Such falsification test requires sampling models from the prior, running the forward simulator and testing whether the data is an outlier with respect to the simulated data. Figure 3 shows the application of the falsification test on the two-panel case. The prior is taken to be a wide uniform prior. Samples of θ and φ are sampled following the hierarchical framework and the simulated data is generated by forward modeling. We use a Robust Mahalanobis Distance test to define whether the data is an outlier with respect to the simulated data samples. Figure 3 shows this is not the case.

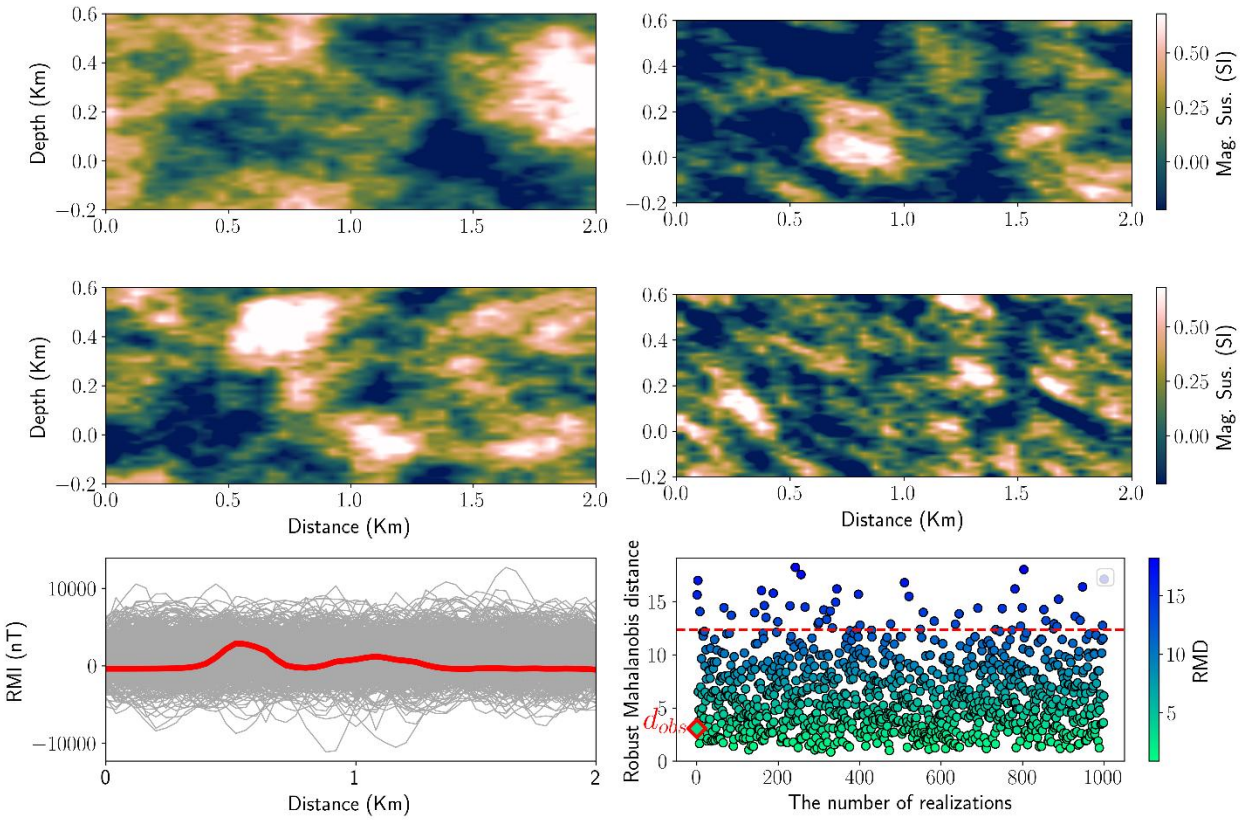

Figure 3: four realizations of magnetic susceptibility with different mean and covariance. Bottom: the red line is the actual observed magnetic data, the dark grey lines the forward simulated data. On the right is the comparison, in terms of robust Mahalanobis distance [13,14], between the observed data and the simulated data.

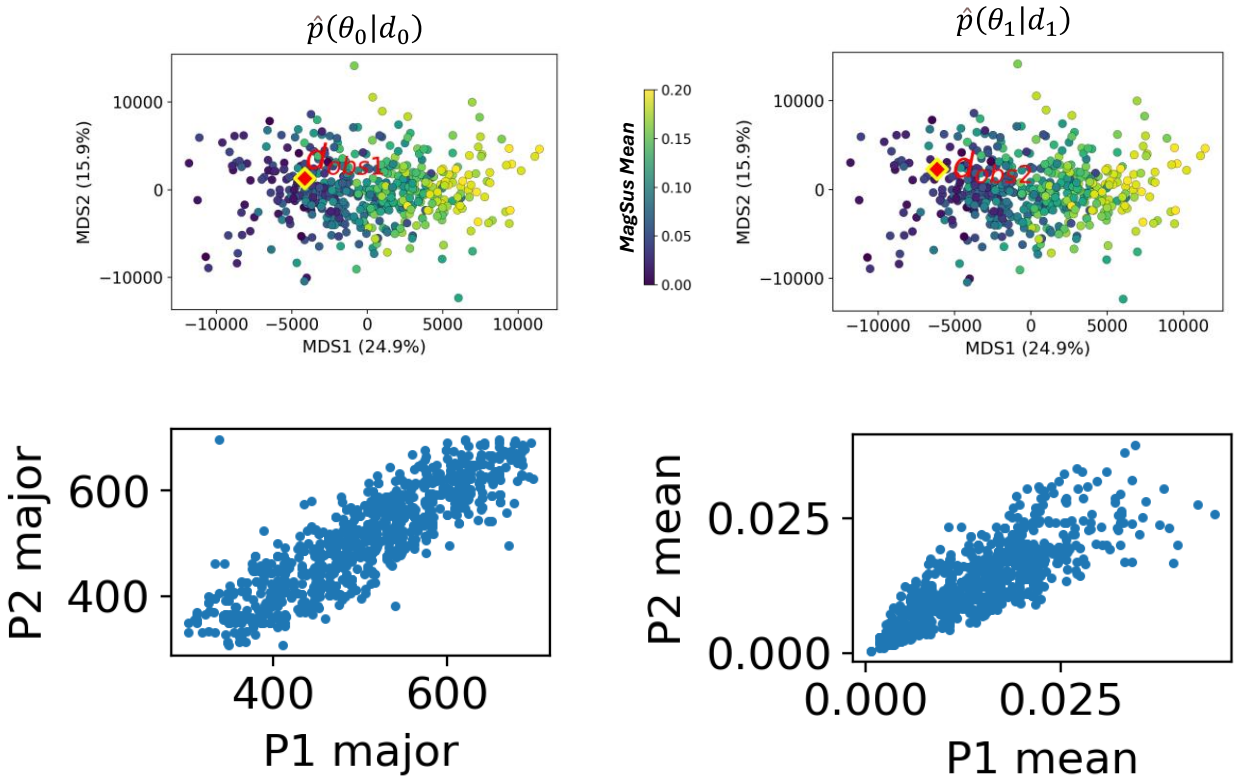

Figure 4: (top) geophysical data mapped into a two-dimensional space using multidimensional scaling: what is shown are the forward simulated data as well as the observed data from panel 0 and 1 (bottom) the relationship between major range and mean of two consecutive panels

4.1.2. Estimate predictive models for Gaussian process hyperparameters $\hat{p}(\theta|d), p^*(\theta_{i+1}|\theta_i)$.

Figure 4 shows the various steps to estimate, then sample from $p^*(\theta_{i+1}|\theta_i)$. First, the data are reduced in dimension using MDS (multi-dimensional scaling). In this case, the first five principal components contain more than 95% of variance. The dimensional of θ is five, so a total of 10 dimensions cover the hyper-parameter and data variables. Figure 4 shows a projection into 2D data (first two principal directions for d) and 1D parameter (mean). The pdfs $\hat{p}(\theta|d)$ are estimated using kernel density estimation. Figure 4 shows the resulting correlation between the mean and the major range. Clearly, a correlation exists between hyper-parameters of two consecutive panels.

4.1.3. Predict & Filter

Panel P_0 needs to be inverted from the geophysical data above that panel. This requires first sampling $\theta_0 \sim \hat{p}(\theta_0|d_{obs,0})$, then performing probability perturbation (Appendix A) on the first panel using a Gaussian process with hyper-parameters θ_0. Figure 5 shows four initial realizations sampled from the prior. The second row shows four realizations with hyper-parameters sampled from $\hat{p}(\theta_0|d_{obs,0})$. Each realization is then perturbed using GDM method to achieve models that match the observations, see the bottom two rows in Figure 5.

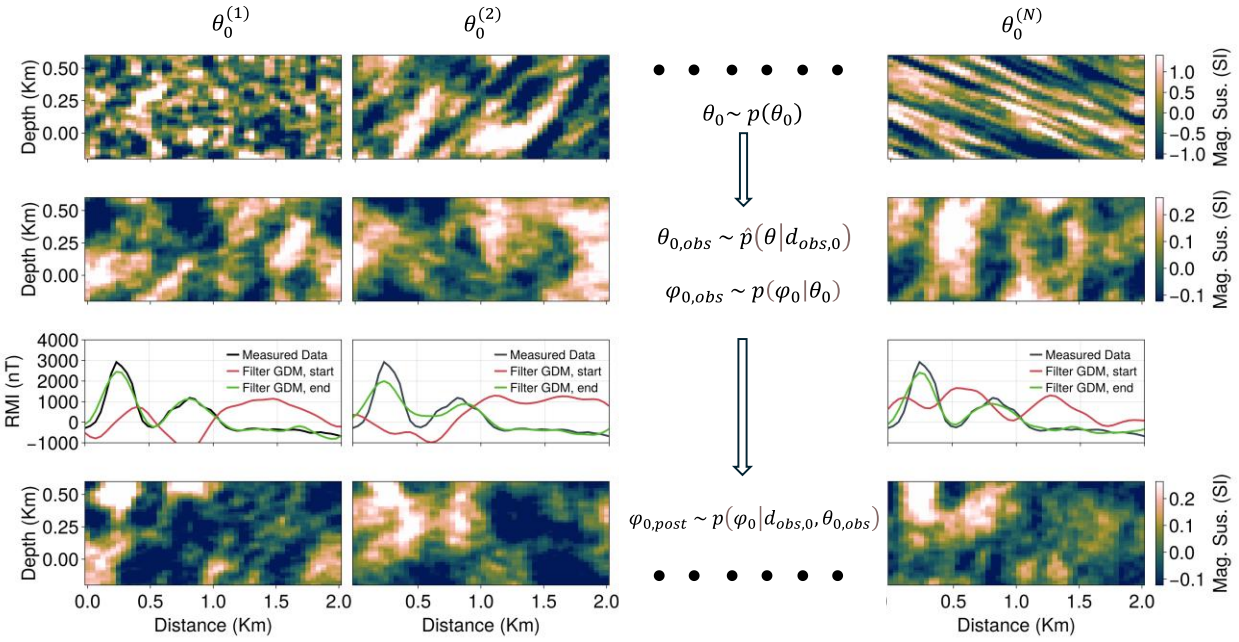

Figure 5: procedure for the first panel: (row 1) sample hyperparameters from the prior (row 2) update hyper-parameters using the observed magnetic data, (row 3) comparison between observed data, simulated data before GDM, and simulated data after GDM (row 4) posterior models for the first panel.

The next step is the prediction step of the next panel P_1, see Figure 6. In this step we first sample $\theta_1 \sim p^*(\theta_1|\theta_0)$, then sample realization of panel 1, constrained (conditioned) to the magnetic susceptibility of the previous panel. These realizations are the new predictive distribution that goes into the gradual deformation method to generate P2 models that match the data. This procedure is iterated if more panels need to be inverted.

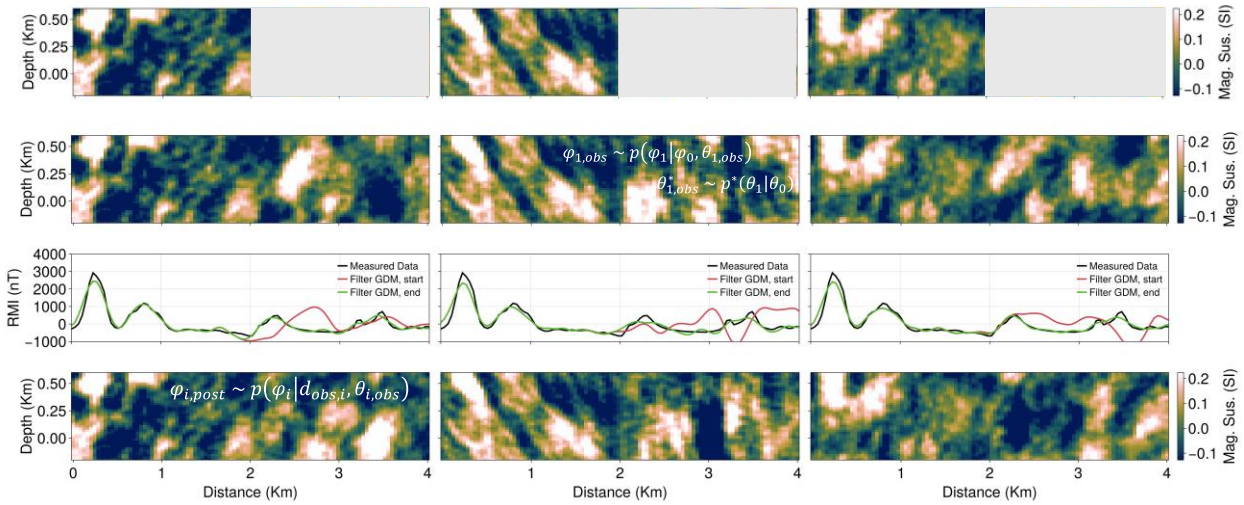

Figure 6: iteration to the next panel P1 (first row) results from previous iteration, (row two) prediction if the next panel given the previous panel for both hyperparameters and Gaussian model realization (row three) comparison of mismatches, (row four) posterior for the next panel filtered using the gradual deformation method.

4.2. Four panel case: uncertainty analysis

Figure 7 shows three realizations of the full 4 panel case, together with the ensemble mean and ensemble variance. Because of the averaging, the ensemble mean loses spatial correlation that might exist and represents a smooth model (much like a deterministic inversion). The ensemble variance can be seen as one metric that characterizes uncertainty (but not the only one). We observe here that the variance increases with depth, but not uniformly. For example, the area in the first 1km has much higher uncertainty (and higher mean) than the rest of the panel.

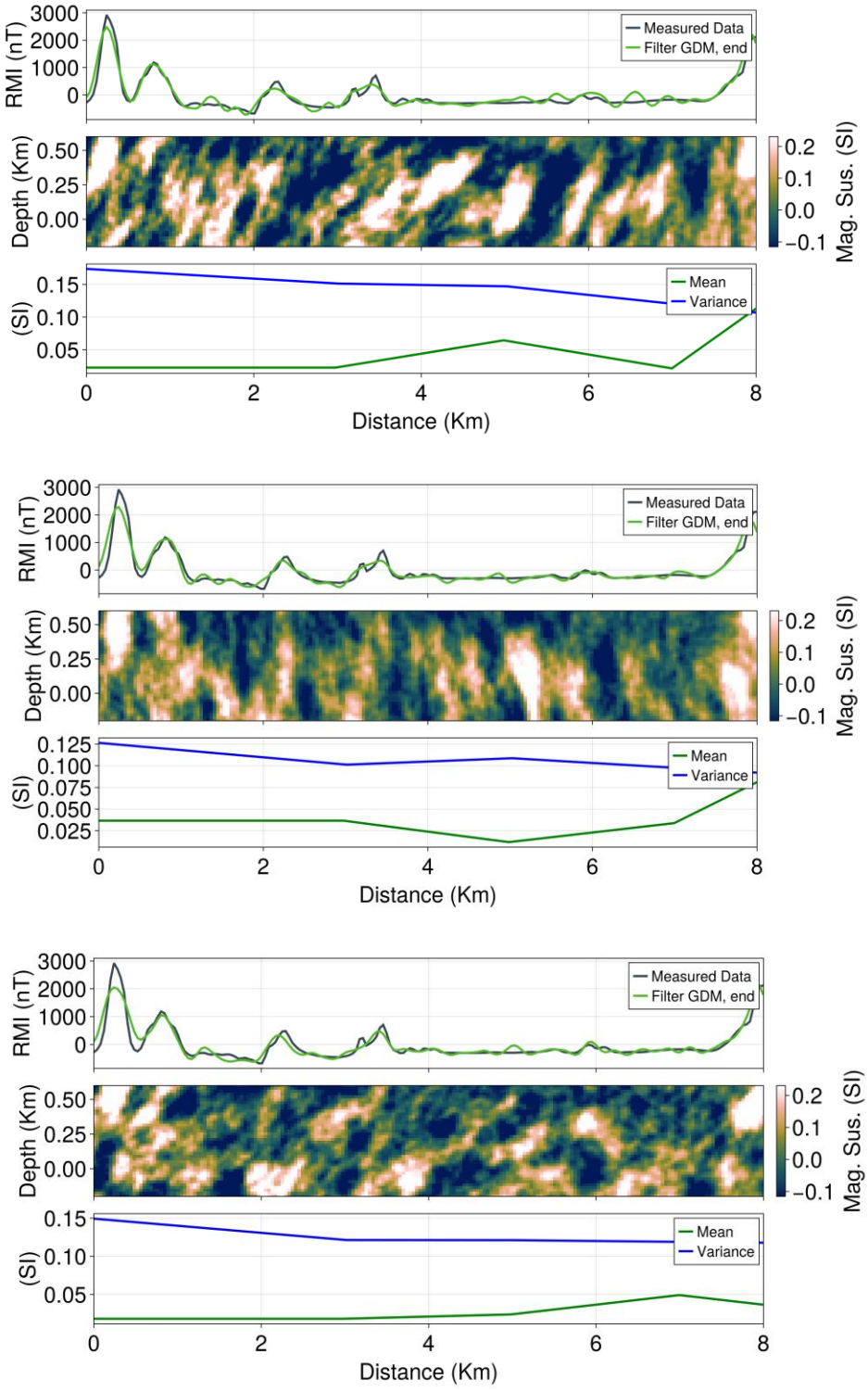

Figure 7: three inverted magnetic susceptibility models; shown are the matches as well as the variation of the mean and variance of the magnetic susceptibility used in the inversion.

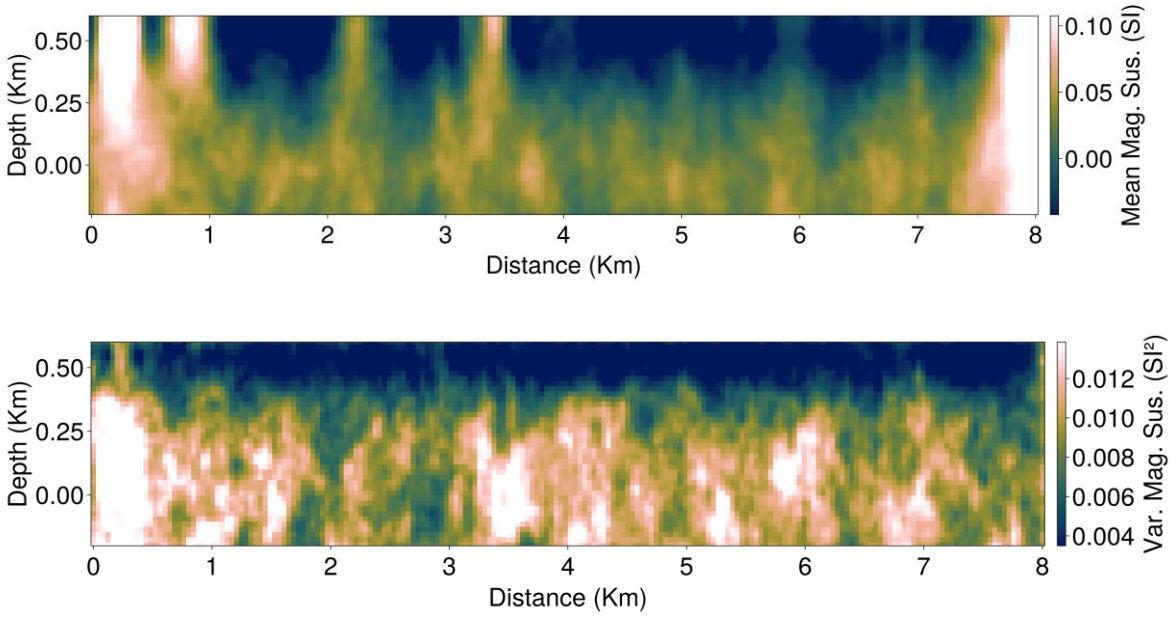

Figure 8: (top) mean of the ensemble of the inverted models, (bottom) variance of the ensemble

4.3. Uncertainty quantification with multiple parallel panels

We ran the same procedure on four parallel lines each with 4 panels, see Figure 1. Since we have many realizations, we can also calculate probabilities per each line. For example, in Figure 9 we plot the probability that the magnetic susceptibility is above 0.039 (which is the 75% quantile of the inverted magnetic susceptibility). High probability means high likelihood of exceeding this threshold. One observes clearly high likely high magnetic features occurring in the domain. The results can be used by geologists/geophysicists for further interpretation of what these features mean and how they are to be connected in 3D.

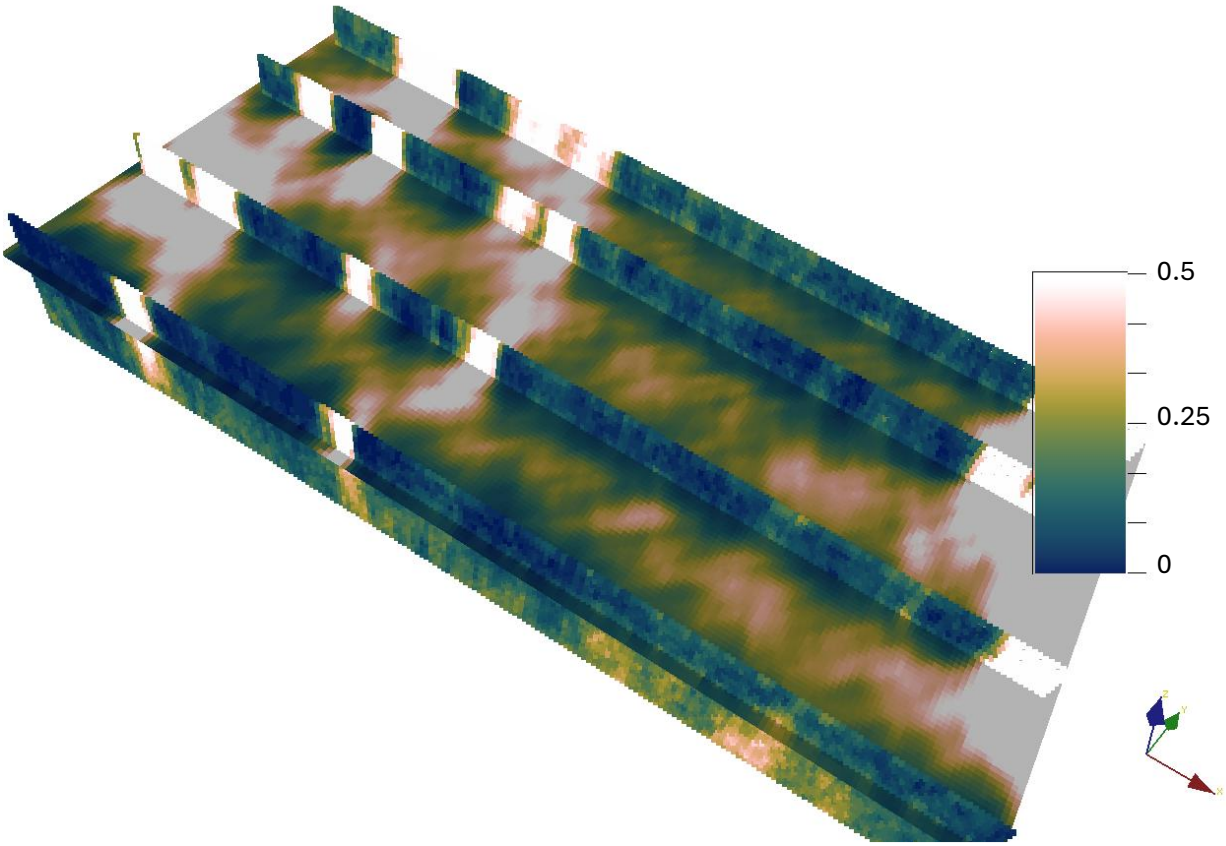

Figure 9: Probability for magnetic susceptibility to be above 0.039, calculated from multiple realizations and interpolated in 3D using Gaussian Process Regression (Müller et al., 2022)

5. Discussion

Choosing a prior model for inversion is challenging, and then using such prior model in the inversion is equally challenging. In this paper, we introduce a non-stationary Gaussian process prior model that provides compromises on both challenges. This Gaussian prior has the flexibility to match data well because the mean and covariance terms are considered uncertain, in addition to the spatial uncertainty of a petrophysical property. Gaussian models can easily be simulated in sequences of panels without artifacts, thereby making large-scale inversion possible. Additionally, many inversion algorithms exist for Gaussian priors. We used the probability perturbation method, but anyone's favorite method can be used as well. The compromise lies in the fact the Gaussian prior cannot capture more complex and detailed geological variability such as faulting, stratigraphy, and other discrete features. Our procedure includes a falsification test to investigate

if the Gaussian prior should be rejected, which may be the case with significant discrete changes in the data.

However, we believe it is a step forward in the context of mineral exploration where the common practice is to first perform a deterministic smooth geophysical inversion, then only do manual interpretation of the results. Such manual interpretation may however be biased because deterministic inversion may ignore important sources of variability, as we have shown through the multitude of inversion that match the data that look very different from a deterministic inversion. As a result, planning drilling based on deterministic inversion only may miss the very magnetic anomaly one wants to target. At a minimum this method may help geologists interpret deterministic inversion since now uncertainty is quantified. The latter is very useful to avoid overinterpreting detailed features of the deterministic inversion. A probability model such as shown in Figure 9 will help in avoiding such overinterpretation.

The proposed approach has a remarkably small computational footprint. The GDM iterations and panels along a flightline are computed sequentially and on a single thread. The method scales through parallelization at the level of independent realizations. Per-realization memory is on the order of 1.1 GB, so an ensemble of 100 realizations occupies approximately 110 GB of RAM and fits comfortably on a single multi-core workstation. On the AMD EPYC 7713 used for our experiments, with 64 physical cores and 128 hardware threads, the per-panel cost is dominated by the 150 GDM outer iterations needed to converge to a data-matching realization. A single realization spanning four panels completes in 45 min to 1 hour, and because the 100 realizations run concurrently, the full ensemble completes in essentially the same wall-clock. The wall-clock scales linearly with the length of the flightline. Ensemble-based stochastic inversion at the line scale therefore runs on a single workstation in under an hour.

Because of its flexibility, the methodology can be extended. For example, one may invert 3D blocks instead of panels and perform inversion of such blocks in a sequence such that a very large area is covered in 3D. The method can be extended to multi-physics inversion by adding a model

of co-variation between two or more petrophysical properties. Several such models are available for Gaussian processes in the geostatistical literature (i.e. Verly 1993; Sabeti et al., 2017; Erten, O., & Deutsch 2021).

6. Conclusions

An increase in the demand for critical minerals will necessitate the acquisition and inversion of massive amounts of geophysical data. In terms of inversion the focus so far has mostly been on large scale deterministic inversion, or local scale stochastic inversion. Large-scale stochastic inversion, producing multiple models of petrophysical properties, has not yet been achieved. In this paper, we present a methodology that makes a step in that direction. Our methodology implements a sequential Bayesian inversion of blocks of data while avoiding the creation of artifacts at the block boundaries. The latter is achieved by formulating the prior distribution models as a non-stationary Gaussian process that is sequentially simulated from block to block. The filtering step is achieved by means of the probability perturbation method that inverts each block locally. The resulting uncertainty quantification may help geologists interpret the variation in 3D. Having knowledge of uncertainty may prevent overinterpreting variation in the inversion that is a risk with traditional deterministic inversion

Author Contributions

All authors contributed to defining the problem and to the study's conception and design. Conceptualization, J.K.C. and D.Z.Y.; Methodology, J.K.C., D.Z.Y., J.P.D., J.K. and C.S.; Software, J.K., J.P.D. and D.Z.Y.; Validation, J.K.C., D.Z.Y., P.L., J.P.D. and J.K.; Formal analysis, J.P.D., P.L., J.K. and D.Z.Y.; Investigation, J.P.D., P.L., J.K. and D.Z.Y.; Resources, J.K.C.; Data curation, J.P.D. and P.L.; Writing—original draft, J.K.C.; Writing—review & editing, C.S., P.L., J.P.D., J.K. and D.Z.Y.; Visualization, J.P.D., J.K., P.L., D.Z.Y. and J.K.C.; Supervision, J.K.C., C.S. and D.Z.Y.; Project administration, D.Z.Y.; Funding acquisition, J.K.C. All authors have read and agreed to the published version of the manuscript.

Funding

This research received no external funding

Data Availability Statement

The HeliTEM airborne magnetic data analyzed in this study are publicly available through the Geomining Information System of Quebec (assessment work GM 72975) at https://gq.mines.gouv.qc.ca/documents/EXAMINE/GM72975, released to the public domain by KoBold Metals (Szentesy, 2022). The methodology, including the sequential Bayesian framework, the gradual deformation method, and the probability perturbation method, is fully described in the manuscript and Appendix A; underlying Gaussian process simulation routines are available through the open-source GeoStats.jl package (Hoffimann, 2018). The inverted realizations generated for this study are not retained and are therefore not available for redistribution; however, they can be reproduced from the publicly available input data using the methodology described herein.

Acknowledgments

The authors gratefully acknowledge KoBold Metals for releasing the HeliTEM survey data into the public domain, Xcalibur Smart Mapping for the airborne data acquisition, and the Government of Québec (Geomining Information System) for hosting and curating the public dataset. The

authors also acknowledge the Stanford Intelligent Systems Lab (SISL) for providing the computational resources used in this study. We also would like to acknowledge the affiliate members of Stanford Mineral-X for supporting this research, including KoBold Metals, Birdra, Ero Copper, Fleet Space Technologies, Ideon Technologies, Xcalibur, and Edra Labs.

Conflicts of Interest

The authors declare no conflict of interest.

7. References

1. Mulè, S.; Soerensen, C.; Munday, T. Handling Noise in AEM Inversion – Implications for Subsurface Characterisation. *ASEG Extended Abstracts* **2019**, *2019*, 1–4, doi:10.1080/22020586.2019.12073183.
2. Vallée, M.A.; Smith, R.S. Inversion of Airborne Time-domain Electromagnetic Data to a 1D Structure Using Lateral Constraints. *Near Surface Geophysics* **2008**, *7*, 63–71, doi:10.3997/1873-0604.2008035.
3. W. Oldenburg, D.; Haber, E.; Napier, S.; Shekhtman, R. 3D Inversion of Time Domain Data with Integrated Application to Mineral Exploration.; European Association of Geoscientists & Engineers, 2007.
4. Oldenburg, D.W.; Pratt, D.A. Geophysical Inversion for Mineral Exploration: A Decade of Progress in Theory and Practice. In Proceedings of Exploration (Vol. 7, No. 5, Pp. 61-95). **2007**, *Vol. 7, No. 5, pp. 61–95*.
5. Engebretsen, K.W.; Zhang, B.; Fiandaca, G.; Madsen, L.M.; Auken, E.; Christiansen, A.V. Accelerated 2.5-D Inversion of Airborne Transient Electromagnetic Data Using Reduced 3-D Meshing. *Geophysical Journal International* **2022**, *230*, 643–653, doi:10.1093/gji/ggac077.
6. Zhdanov, M.S.; Wan, L.; Jorgensen, M. Joint Three-Dimensional Inversion of Gravity and Magnetic Data Collected in the Area of Victoria Mine, Nevada, Using the Gramian Constraints. *Minerals* **2024**, *14*, 292, doi:10.3390/min14030292.
7. Munch, F.D.; Grayver, A. Multi-Scale Imaging of 3-D Electrical Conductivity Structure under the Contiguous US Constrains Lateral Variations in the Upper Mantle Water Content. *Earth and Planetary Science Letters* **2023**, *602*, 117939, doi:10.1016/j.epsl.2022.117939.
8. Mancinelli, P.; Pauselli, C.; Fournier, D.; Fedi, M.; Minelli, G.; Barchi, M.R. Three Dimensional Gravity Local Inversion Across the Area Struck by the 2016–2017 Seismic Events in Central Italy. *Journal of Geophysical Research: Solid Earth* **2020**, *125*, doi:10.1029/2019jb018853.
9. Szentesy, Z. *Geophysical Survey Report, Airborne Magnetic and Helitem2 Survey, Cape Smith Belt Project 2100109B. 9414-5349 QUEBEC INC, Assessment Work Submitted to the Government of Québec. GM 72975, 70 Pages. Available at Https://Gq.Mines.Gouv.Qc.ca/Documents/EXAMINE/GM72975.*; 2022;
10. Hoffimann, J. GeoStats.Jl – High-Performance Geostatistics in Julia. *Journal of Open Source Software* **2018**, *3*, 692, doi:10.21105/joss.00692.

11. Oliver, D.S. Moving Averages for Gaussian Simulation in Two and Three Dimensions. *Mathematical Geology* **1995**, *27*, 939–960, doi:10.1007/bf02091660.
12. Ravalec, M.L.; Noetinger, B.; Hu, L.Y. The FFT Moving Average (FFT-MA) Generator: An Efficient Numerical Method for Generating and Conditioning Gaussian Simulations. *Mathematical Geology* **2000**, *32*, 701–723, doi:10.1023/a:1007542406333.
13. Hubert, M.; Debruyne, M. Minimum Covariance Determinant. *WIREs Computational Statistics* **2009**, *2*, 36–43, doi:10.1002/wics.61.
14. Yin, Z.; Strebelle, S.; Caers, J. Automated Monte Carlo-Based Quantification and Updating of Geological Uncertainty with Borehole Data (AutoBEL v1.0). *Geoscientific Model Development* **2020**, *13*, 651–672, doi:10.5194/gmd-13-651-2020.
15. Scheidt, C.; Li, L.; Caers, J. *Quantifying Uncertainty in Subsurface Systems*; Geophysical Monograph Series; John Wiley & Sons, 2018; ISBN 978-1-119-32587-1.
16. Caers, J.; Hoffman, T. The Probability Perturbation Method: A New Look at Bayesian Inverse Modeling. *Math Geol* **2006**, *38*, 81–100, doi:10.1007/s11004-005-9005-9.
17. Hu, L.Y. Gradual Deformation and Iterative Calibration of Gaussian-Related Stochastic Models. *Mathematical Geology* **2000**, *32*, 87–108, doi:10.1023/A:1007506918588.
18. Hu, L.Y.; Blanc, G.; Noetinger, B. Gradual Deformation and Iterative Calibration of Sequential Stochastic Simulations. *Mathematical Geology* **2001**, *33*, 475–489, doi:10.1023/A:1011088913233.
19. Caers, J. Comparing the Gradual Deformation with the Probability Perturbation Method for Solving Inverse Problems. *Mathematical Geology* **2007**, doi:10.1007/s11004-007-9119-3.
20. Hu, L.Y. Extended Probability Perturbation Method for Calibrating Stochastic Reservoir Models. *Mathematical Geosciences* **2008**, *40*, 875–885, doi:10.1007/s11004-008-9158-4.

Appendix A: Solving a non-linear inverse problem using a Gaussian prior

A.1. Generating correlated samples from a univariate distribution

Solving inverse problems that involve spatial models is challenging, because of the high dimensionality of the model and the difficulty of creating perturbation mechanisms consistent with a prior distribution. For example, in an McMC sampler of the posterior one would need to design a proposal distribution that 1) generate a proposal spatial model, 2) respect the spatial correlation imposed in such spatial model. In the case of a Gaussian process prior, this means that any perturbation of the model still needs to be a sample of those same Gaussian priors. Several methodologies have been proposed (see Chapter 6, [15]). In our work we will use the gradual deformation method (GDM) and probability perturbation method (PPM) [16–18].

To present these methods, we consider first a simple example, namely that of sampling from the exponential distribution

$$u = F(x) = P(X \leq x) = 1 - \exp(-\lambda x) \tag{A1}$$

The quantile function is known analytically

$$x = Q(u) = -\frac{1}{\lambda} log(1 - u) \tag{A2}$$

Hence exact sampling is possible. Naïve Monte Carlo generates independent draws from this distribution. Let's now consider a sampling scheme where draws are no longer independent, but with serial correlation, yet still samples of the same exponential distribution. In an independent draw we sample two independent values u_1 and u_2, then evaluate the quantile function. Now we would like u_2 to be small perturbation u_1, hence x_1 is a small perturbation of x_2. To do this we need to be able to generate correlated draws from the uniform distribution. We first consider a standard Gaussian distribution and make correlated draws from that distribution, then perform a rank-preserving transformation of the Gaussian draws into draws u. We do it this way because there is a simple way to generate correlated Gaussian draws. Namely, consider a standard Gaussian draw y_1, then draw a second, independent draw y_2 and calculate the following value

$$y(r) = y_1 \cos(r) + y_2 \sin(r)$$

(A3)

when $r = 0$, then $y(r) = y_1$ and when $r = \pi/2$, $y(r) = y_1$. Also, no matter what value r has, $y(r)$ is always standard Gaussian, namely

$$E[Y(r)] = cos(r)E[Y_1] + sin(r)E[Y_2] = 0$$

$$Var\big(Y(r)\big) = E[(Y(r) - 0)^2] = \cos^2(r)\, var[Y_1] + sin^2(r)\, var[Y_2] = 1$$

(A4)

Therefore $Y(r)$ represent a gradual perturbation between two independent draws y_1 and y_2. The gradual deformation algorithm iterates these perturbations between different Gaussian draws, each time these Gaussian draws can be transformed into uniform draws using the Gaussian quantile function

$$u(r) = G\big(y(r)\big) \sim U[0,1]$$

(A5)

Gradual deformation method

Input: $u_0 \sim Uniform(0,1)$; Δr; $\lambda =$ mean of the exponential distribution

Output: Correlated draws of $P(X \leq x) = 1 - \exp(-\lambda x)$

```
for i = 1, ..., N
        u_i ~ Uniform(0,1)
        y_i = G^{-1}(u_i)
        for r = -π, π with steps Δr
                y(r) = y_{i-1} cos(r) + y_i sin(r)
                u = G(y(r))
                return: x = -1/λ log(1 - u)
        end
end
```

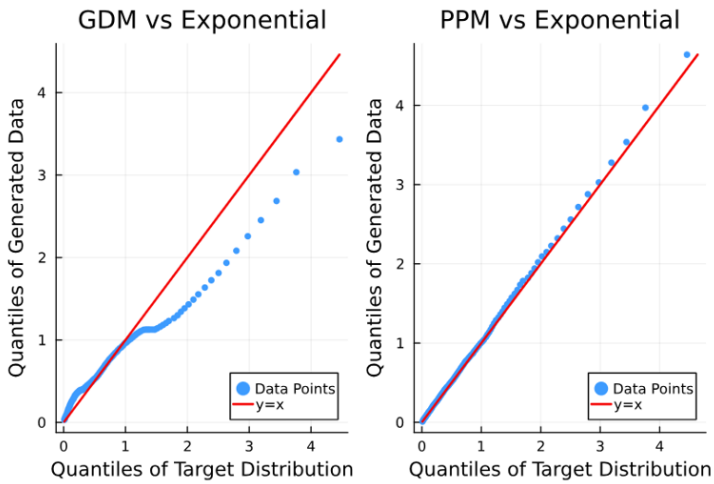

Figure A.1: Comparing naïve monte Carlo with (left) gradual deformation-based sampling of the exponential distribution, (right) probability perturbation.

In Figure A1, we compare the gradual deformation samples of the exponential distribution with the naïve Monte Carlo. The QQ-plot shows however some deviation from the exponential distribution. This issue was discussed in [19], and attributed to the fact that successive linear combinations eventually leads to a deviation from the target Gaussian (or uniform distribution).

A solution to this was suggested in [20] relying on an extension of the probability perturbation method. Now, we do not work by perturbing individual samples, but by perturbing the probability from which samples are drawn. For example, suppose we'd like to generate samples from the Bernoulli distribution with probability p, then naïve Monte Carlo method to sample i is

$$u \sim uniform(0,1);\ \ if(u \leq p)\ i = 1, else\ i = 0 \tag{A6}$$

If we would like to generate correlated draws of 0's and 1's but that have the same p, then we make the next draw of I, namely i^n dependent on the previous draw i^{n-1} by sampling from a perturbed p (REF)

$$p_{perturbed} = r\ p + (1 - r)\ i^{(n-1)} \tag{A7}$$

If $r = 1$, then a new independent sample is drawn, for $r = 0$, the same value is drawn, but the expected value is still p

$$E[I = 1] = rp + (1 - r)E[I = 1] = p$$

(A8)

While GDM is an algorithm, PPM starts with probability theory principles and a proof that properties such as expected value are preserved. PPM has been extended to generate correlated draws from any univariate distribution F with quantile function Q (such as the exponential distribution). In this extension p in Eq. (A7) is replaced by $F(x)$. We define the perturbed cdf:

$$F_{perturbed}(r, x, x_0) = (1 - r)1_{x>x_0} + rF(x)$$

(A9)

x_0 is the initial draw. Figure provides a practical algorithm

Probability Perturbation Method

Input: Δr; x_0

Output: Correlated draws of $F(x)$

$u_0 = F(x_0)$

$for\ i = 1, \dots, N$

$u \sim Uniform(0,1)$

$for\ r = 0,1$ with steps Δr

$if\ u_0 r < u < 1 - r + ru_0$

$x = x_0$

$else\ if\ (u \leq r\ u_0)\ \ then$

$x = Q\left(\frac{u}{r}\right)$

$else\ if\ (u \geq 1 - r + ru_0)\ then$

$x = Q\left(\frac{u+r-1}{r}\right)$

$end\ if$

```
            return: x
        end
    end
```

A.2. Generating correlated samples from a mixture model

Consider now the situation where the parameter of the exponential λ itself is uncertain, and has its own distribution, hence the definition of the distribution is

$$f(x,\lambda) = f(\lambda)f(x|\lambda)$$

This situation is similar to the hierarchical model of Figure 2. In this case, sampling is done sequentially

$$\lambda \sim f(\lambda), \text{ then } x \sim f(x|\lambda)$$

To do this, we need two uniform random draws, u_λ and u_x, hence now the gradual deformation equation or probability perturbation is applied to the vector $[\,u_\lambda\; u_x]^T$. Once a perturbed $u_\lambda(r), u_x(r)$ are sampled, they are used to sample a new λ, x. Note that we use the same r to perturb both λ and x jointly:

$$u_0 = F(x_0) \text{ with } u_{0,\lambda} = F_\lambda(\lambda_0);\; u_{0,x} = F_x(x_0)$$

and have the "if then else" for both λ and x, but with the same r.

In Figure A2, an example is shown for the case when

$$f(\lambda) = \exp(-x)\,;\; f(x|\lambda) = \lambda \exp(-\lambda x)$$

In that case, the marginal in x equals

$$f(x) = \int_0^\infty f(x,\lambda)d\lambda = \exp(-x)$$

When performing PPM by both perturbing λ and x, we should obtain two exponential distribution which is confirmed in Figure A2.

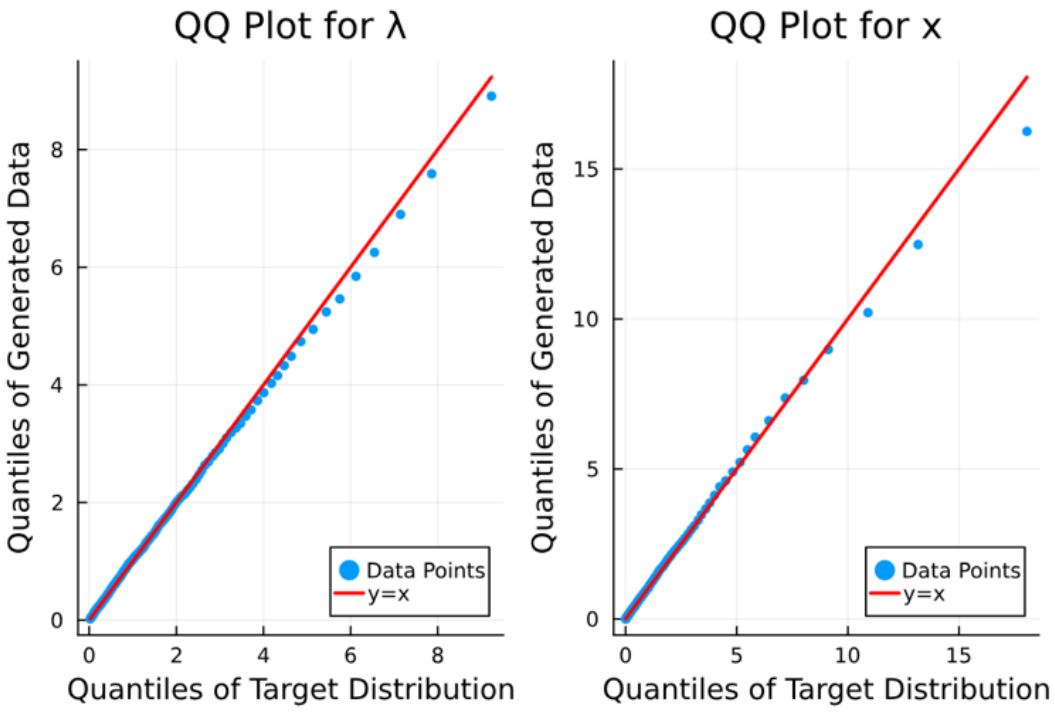

Figure A2: Samples of the x and λ, generated using PPM in the case of exponential priors for both.

A.3. Geophysical inversion with a Gaussian prior using GDM or PPM

The above method provides correlated draws from any univariate distribution, continuous or discrete. This idea can be extended to correlated draws from any high-dimensional distribution, if an algorithm to sample from such high-dimensional distribution is available. Consider for example the implementation of sampling a Gaussian process on a 2D grid, with given mean and covariance function, using the LU decomposition:

Sampling a Gaussian Process using LU decomposition Input: $mean\ \mu, covariance\ function/kernel\ C(h)$ Output: a single sample $\boldsymbol{x}$ of the $GP(\mu, C(h))$ on a $N \times N$ grid	
$C \leftarrow C(h)$	Use covariance function to generate a covariance matrix of size $N^2 \times N^2$

$C = LU$	Cholesky decomposition
$\boldsymbol{u} \sim Uniform(0,1)$	Generate N^2 uniform random values
$\boldsymbol{y} = F^{-1}(\boldsymbol{u})$	Calculate N^2 standard Gaussian random values
$\boldsymbol{x} = \mu + L\boldsymbol{y}$	Convert independent $\boldsymbol{y}$ into dependent $\boldsymbol{x}$

This algorithm generates a vector or independent Gaussian deviates $\boldsymbol{y}$. To perturb $\boldsymbol{x}$, we therefore create perturbations of $\boldsymbol{y}$. An example is shown in Figure A3. Like in the previous section, we can also perturb parameters of the covariance function. In Figure A4 we show such a case where the azimuth angle is uncertain with a uniform distribution between 1 and 180 degrees.

The perturbations can be used in geophysical inversion. For example, in a Bayesian inversion, the PPM can generate new proposal models in a McMC algorithm. The proposal models are always samples from the prior distribution, if the algorithm to sample from the prior is provided (e.g. a Gaussian prior in Figure A3).

The method can also be used in non-Bayesian stochastic inversion by using PPM as an optimizer, which is the application in this paper. The optimization consists of an outer loop and an inner loop, that is visualized in Figure A5. In the outer loop new realizations of the prior are generated by generating new realizations of a unform random vector. In the inner loop the value of r is optimized using a 1D optimization method (such as Dekker-Brent).

Stochastic Inversion using PPM with Gaussian prior
Input: $\boldsymbol{d}_{obs}, mismatch(\boldsymbol{d}_{obs}, \boldsymbol{m}); mean\ \mu; covariance\ C$
Output: inverted model $\widehat{\boldsymbol{m}}$
$\boldsymbol{u}_o \sim Uniform(0,1)$
$\boldsymbol{m}_o = GaussianPriorAlgo(\mu, C, \boldsymbol{u}_o)$
$for\ i = 1, \dots, N_{max}$
$\boldsymbol{u}_i \sim Uniform(0,1)$
$\boldsymbol{u}_{opt} \leftarrow 1D\_optimization(mismatch, \boldsymbol{d}_{obs}, \boldsymbol{u}_i, \boldsymbol{u}_{i-1})$
$\boldsymbol{m}_i = GaussianPriorAlgo(\mu, C, \boldsymbol{u}_{opt})$

end

Return $\hat{\boldsymbol{m}} = \boldsymbol{m}_{N_{max}}$

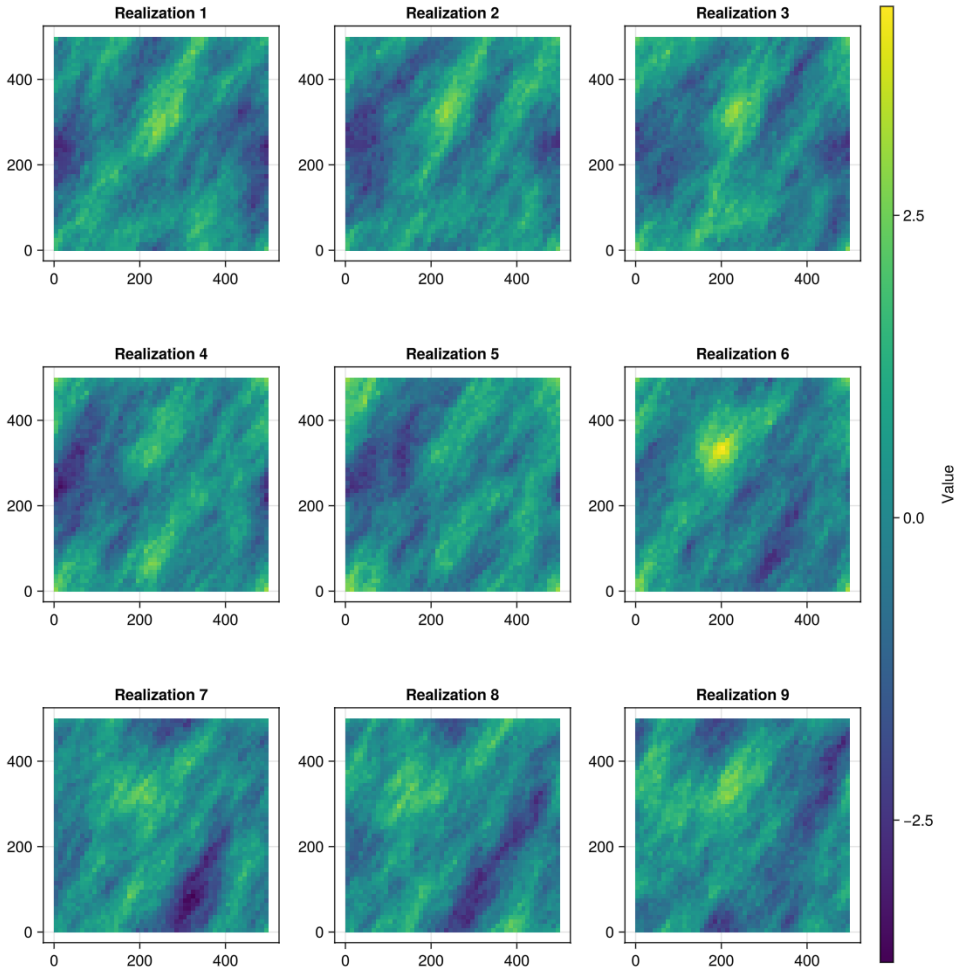

Figure A3: perturbations of Gaussian realizations using PPM, with fixed covariance model

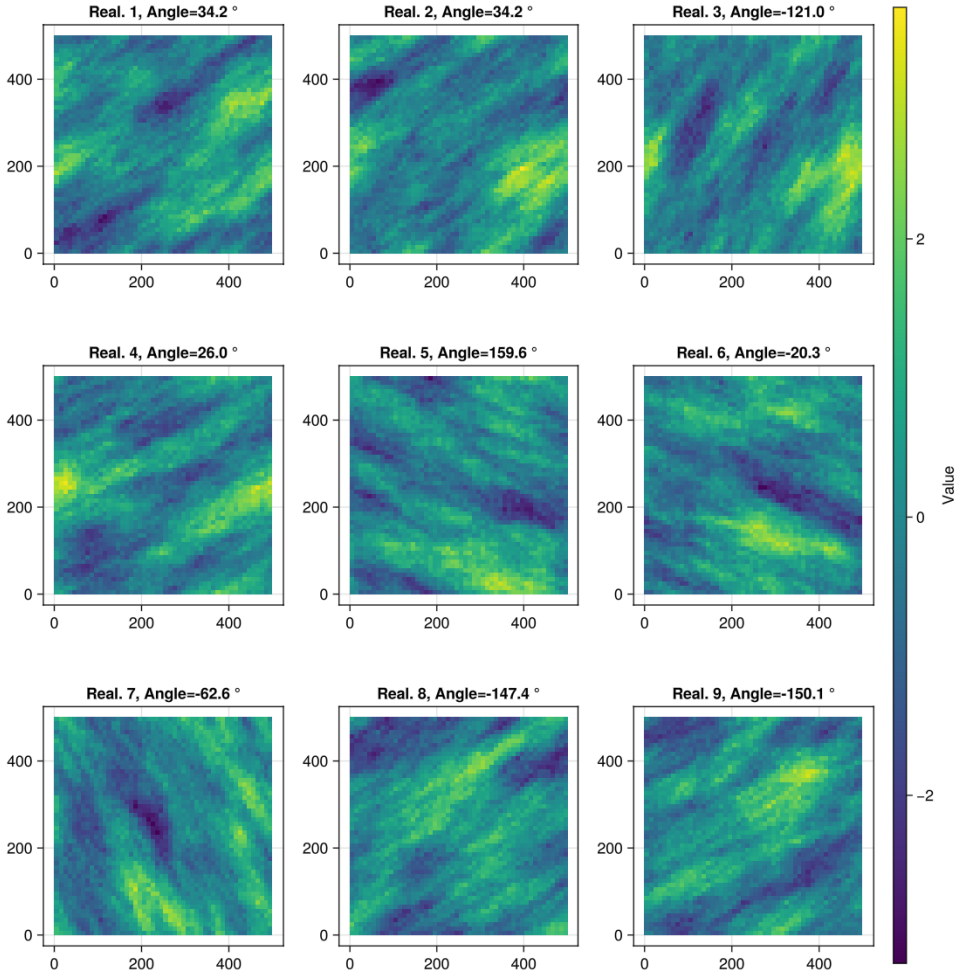

Figure A4: joint perturbation of a Gaussian realization and the azimuth angle of the covariance model.

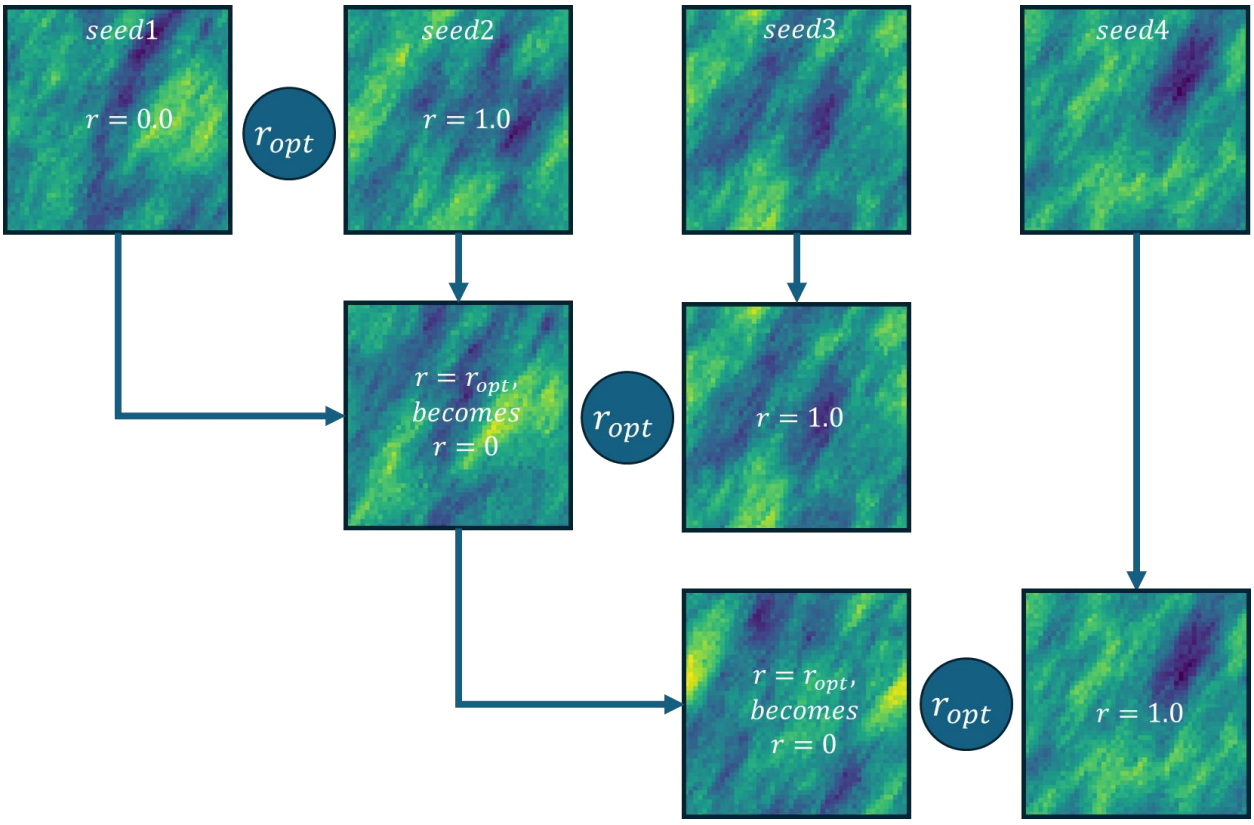

Figure A5: Optimization/Inversion with the PPM/GDM consists of an inner and outer loop.

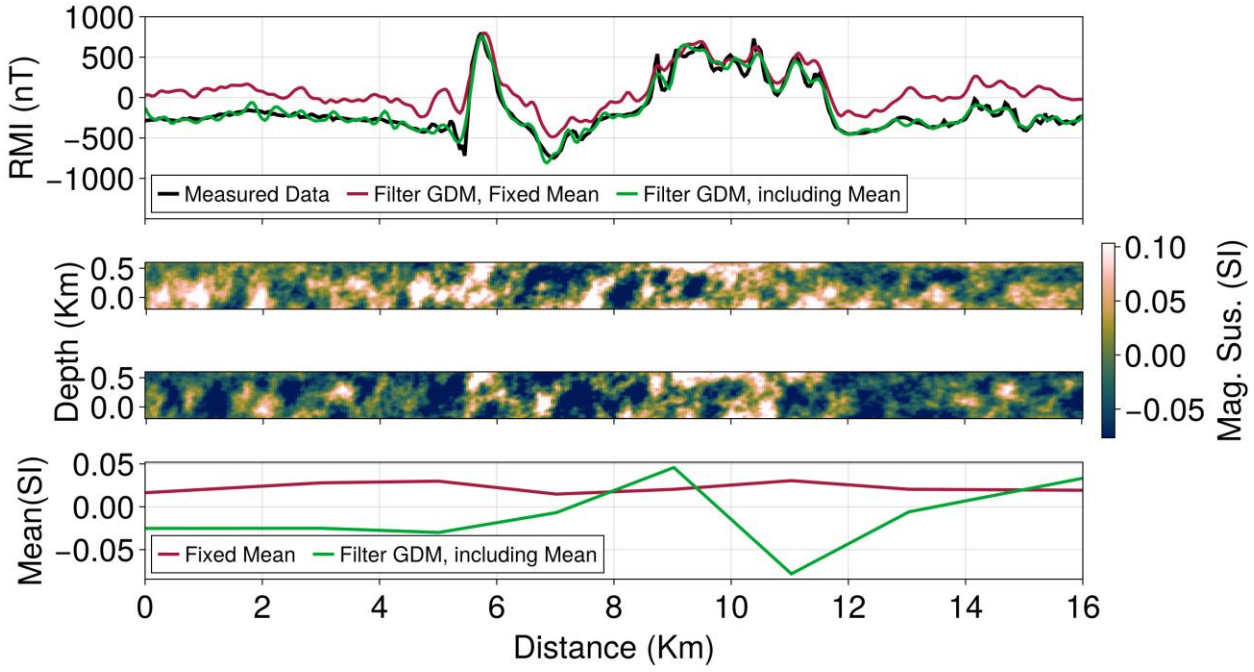

Figure A6: example of perturbing the mean during gradual deformation vs fixing the mean.

In Figure A6 we see the utility of jointly perturbing the mean of each panel as opposed to fixing the mean. When fixing the mean, the PPM algorithm does not converge to a matching solution. When perturbing the mean from $p(\theta|d)$ of Eq (22), with θ the mean we converge to a solution.